

RefFusion: Reference Adapted Diffusion Models for 3D Scene Inpainting

ASHKAN MIRZAEI, NVIDIA, University of Toronto, Canada
 RICCARDO DE LUTIO, NVIDIA, USA
 SEUNG WOOK KIM, NVIDIA, South Korea
 DAVID ACUNA, NVIDIA, Canada
 JONATHAN KELLY, University of Toronto, Canada
 SANJA FIDLER, NVIDIA, University of Toronto, Canada
 IGOR GILITSCHENSKI, University of Toronto, Canada
 ZAN GOJCIC, NVIDIA, Switzerland

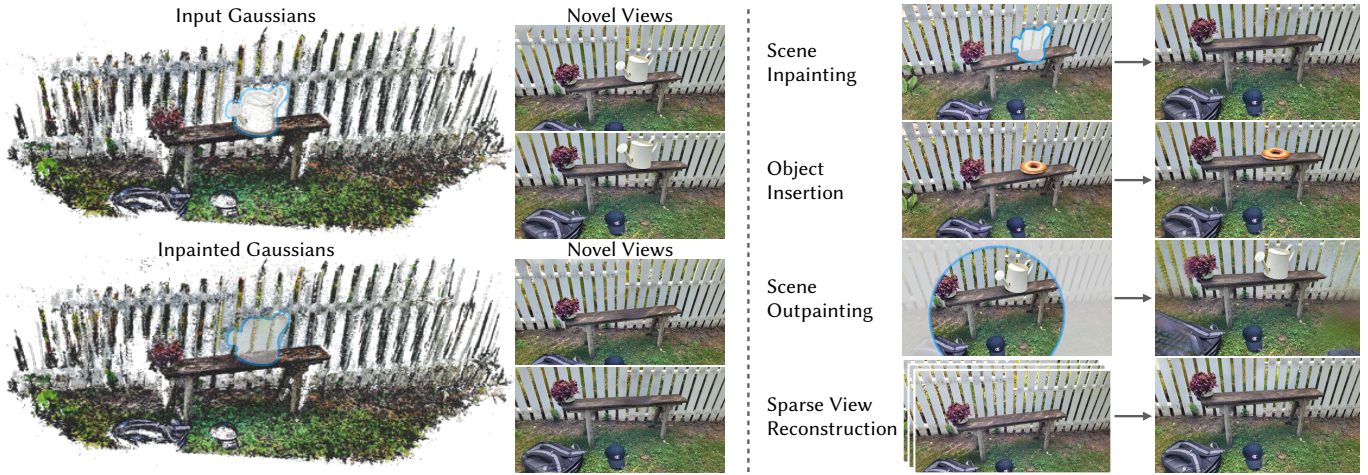


Fig. 1. This work presents an approach for 3D inpainting based on the distillation of the 2D generative priors from reference adapted diffusion models. *Left*: Given a scene represented using 3D Gaussian splatting and the user-defined mask, we use the score distillation objective based on a personalized diffusion model to inpaint the missing content in 3D. *Right*: Our method is general and can be, without any changes, applied to other editing tasks such as object insertion, outpainting, and sparse view reconstruction. Please visit our [project page](#).

Neural reconstruction approaches are rapidly emerging as the preferred representation for 3D scenes, but their limited editability is still posing a challenge. In this work, we propose an approach for 3D scene inpainting—the task of coherently replacing parts of the reconstructed scene with desired content. Scene inpainting is an inherently ill-posed task as there exist many solutions that plausibly replace the missing content. A good inpainting method should therefore not only enable high-quality synthesis but also a high degree of control. Based on this observation, we focus on enabling explicit control over the inpainted content and leverage a reference image as an efficient means to achieve this goal. Specifically, we introduce **REFFUSION**, a novel 3D inpainting method based on a multi-scale personalization of an image inpainting diffusion model to the given reference view. The personalization effectively adapts the prior distribution to the target scene, resulting in a lower variance of score distillation objective and hence significantly sharper details. Our framework achieves state-of-the-art results for object removal while maintaining high controllability. We further demonstrate the

generality of our formulation on other downstream tasks such as object insertion, scene outpainting, and sparse view reconstruction.

1 INTRODUCTION

Neural reconstruction methods enable seamless reconstruction of 3D scenes from a set of posed images. Their simple formulation, high visual fidelity, and increasingly fast rendering make them the preferred representation for a variety of use cases from AR/VR applications to robotics simulation. While these methods enable novel-view synthesis, they are still inherently limited to the content captured in the training data. Yet, to make them useful in practice, it is critical to impart them with editability. One of the key desirable manipulation operations is the ability to remove parts of the scene and substitute them with some desired content. This task, generally known as *3D inpainting*, involves synthesizing plausible content that coherently blends with the rest of the scene when viewed from any angle. Inpainting is an inherently ill-posed problem as there often exist multiple viable approaches to complete the scene. A good inpainting model should therefore also be controllable, such that users can choose the solution that best fits their needs.

Authors' addresses: Ashkan Mirzaei, NVIDIA, University of Toronto, Canada, ashkan@cs.toronto.edu; Riccardo de Lutio, NVIDIA, USA, rdelutio@nvidia.com; Seung Wook Kim, NVIDIA, South Korea, seungwookk@nvidia.com; David Acuna, NVIDIA, Canada, dacunamarrer@nvidia.com; Jonathan Kelly, University of Toronto, Canada, jkelly@utias.utoronto.ca; Sanja Fidler, NVIDIA, University of Toronto, Canada, sfidler@nvidia.com; Igor Gilitschenski, University of Toronto, Canada, igor@gilitschenski.org; Zan Gojcic, NVIDIA, Switzerland, zan.gojcic@gmail.com.

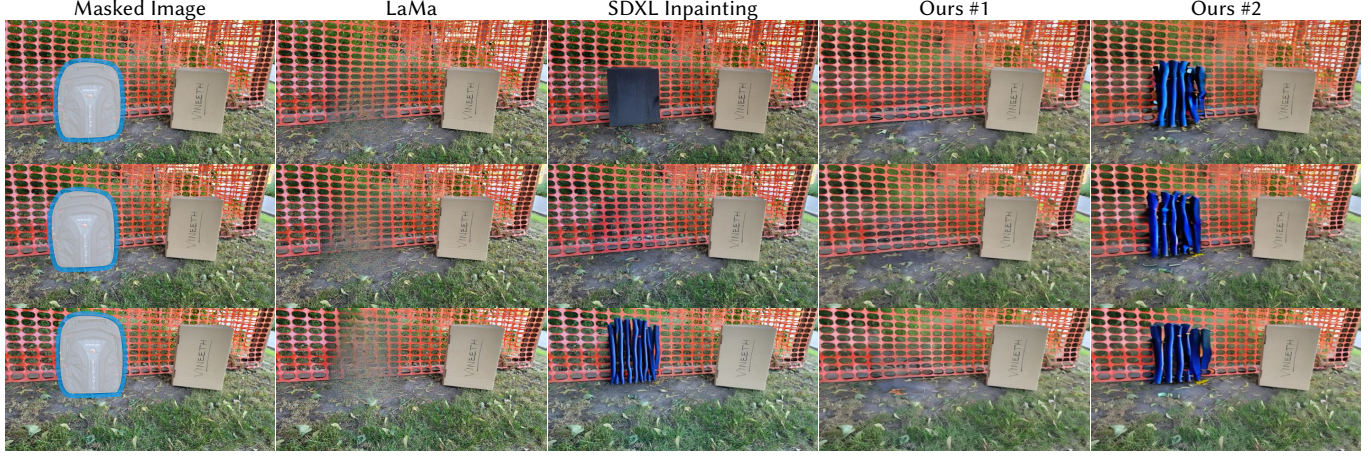


Fig. 2. Comparison of 2D image inpainting methods on multiple views of the same scene. LaMa [Suvorov et al. 2022] yields relatively consistent inpaintings but lacks details. SDXL [Podell et al. 2023] synthesizes content with high-quality, but low multi-view consistency due to the high diversity of its generations. By personalizing the diffusion model to the reference view, our method achieves high-quality generations with superior multi-view consistency. *Ours* #1 and *Ours* #2 are adapted to SDXL outputs shown in the second and third row respectively.

With the advent of large diffusion models [Balaji et al. 2022; Rombach et al. 2022a; Saharia et al. 2022a,b], 2D image inpainting has been getting increasingly close to achieving these properties. Unfortunately, large-scale 3D generative methods still lag far behind. This can be accredited to the lack of large-scale 3D datasets and efficient high-resolution 3D data structures. As a consequence, much of the recent and concurrent work on 3D inpainting has resorted to lifting the priors of 2D inpainting models to 3D. Such lifting is performed either *explicitly*, by independently inpainting one or multiple 2D views and consolidating their multi-view inconsistencies in 3D [Liu et al. 2022; Mirzaei et al. 2023a,b; Wang et al. 2023b]. Alternatively, it can be formulated as a *continuous distillation* process [Poole et al. 2023] that seeks 3D inpaintings using a 2D diffusion model as a prior for optimization [Prabhu et al. 2023].

These methods achieve promising results but many challenges remain: **a) Trade-off between diversity and multi-view consistency.** Deterministic 2D inpainting models, e.g. [Suvorov et al. 2022], yield relatively multi-view consistent inpaintings that can directly be lifted to 3D using perceptual losses [Mirzaei et al. 2023b; Wang et al. 2023b]. Yet, this comes at the cost of diversity and limited visual quality. Prompt-based inpainting diffusion models can synthesize high-quality, diverse, and controllable inpaintings, but due to the loose constraint of text guidance, their inpaintings are highly multi-view inconsistent and thus difficult to lift to 3D (see Figure 2). **b) Maintaining fidelity to the observed content.** By inpainting the 3D content using (inconsistent) 2D masks, these methods ignore that the missing content in 3D is potentially smaller than that naively defined by the 2D masks. For example, in the scene shown in Figure 3, the content behind the vase is observed in other views and therefore does not need to be synthesized. Finally, **c) Conflicting gradients.** The inconsistencies across the inpainted views may lead to conflicting gradients, which in turn result in smoothed-out inpaintings.

To address the above challenges, we propose REFFUSION, a novel 3D inpainting method based on *continuous distillation* of a reference adapted diffusion model. In particular:

i) We propose a multi-scale personalization method for inpainting diffusion models that adapts the model to the given reference view. This contribution alone enables explicit control over the inpainted content and reduces the variance of the score distillation objective. **ii)** We leverage the explicit nature of 3D Gaussian splatting to consolidate noisy 2D masks and direct the gradients of different loss terms to the pertinent regions. **iii)** We propose a combination of objective terms that enables using the SDS optimization procedure at the scene level. **iv)** We propose a new dataset designed for evaluating object removal and 3D inpainting, comprising nine scenes with large camera motion.

The experiments in Section 4 demonstrate the high visual quality, controllability, and diversity of our approach. In addition, the applications in Section 5 showcase the generality of our formulation.

2 RELATED WORK

2D and 3D Inpainting Inpainting is the process of replacing missing regions with realistic content. For example, in 2D this involves producing plausible values for missing pixels of an image. As an inherently generative task, advancements of generative models have led to increased performance of 2D inpainting. Generative Adversarial Network (GAN) [Goodfellow et al. 2014]-based approaches [Li et al. 2022; Liu et al. 2021; Suvorov et al. 2022; Yu et al. 2019; Zhao et al. 2021; Zheng et al. 2022] learn to hallucinate the missing pixels by playing an adversarial game between an image inpainter and a discriminator. Recently, diffusion model (DM) [Ho et al. 2020; Sohl-Dickstein et al. 2015; Song et al. 2021]-based inpainting models [Avrahami et al. 2022; Lugmayr et al. 2022; Meng et al. 2022; Rombach et al. 2022a; Xie et al. 2023] have achieved state-of-the-art results. These operate by gradually perturbing a clean image towards random noise while training a denoising network to reconstruct the image, conditioned on its masked version.

In 3D inpainting, the goal is to synthesize plausible content for the missing regions in 3D scenes. This is a significantly harder task as the generated content needs to be consistent across various views. Although 3D generative models have recently gathered increased

interest [Bautista et al. 2022; Kalischek et al. 2022; Kim et al. 2023; Nichol et al. 2022; Zeng et al. 2022], their quality is still limited by the scarcity of 3D training data and the difficulty of selecting an appropriate underlying representation. Therefore, most existing 3D inpainting models [Haque et al. 2023; Liu et al. 2022; Mirzaei et al. 2023a,b; Prabhu et al. 2023; Wang et al. 2023b; Weber et al. 2023; Weder et al. 2023] still rely on lifting the priors from 2D inpainting models to 3D. In particular, they first inpaint masked input images and complement the reconstruction objective with regularization techniques to lessen the multi-view inconsistencies [Liu et al. 2022; Mirzaei et al. 2023a,b; Wang et al. 2023b; Weder et al. 2023]. The problem of inconsistency is amplified when using recent DM-based inpainting models with increased diversity. We address the challenge with the score distillation objective [Poole et al. 2023] as follows.

Distilling 2D Diffusion Model Priors Score Distillation Sampling (SDS), first introduced by [Poole et al. 2023], has recently been used to generate realistic 3D objects [Chen et al. 2023; Liang et al. 2023; Lin et al. 2023; Wang et al. 2023a] and even 4D scenes [Ling et al. 2023; Ren et al. 2023; Zheng et al. 2023] by distilling the priors of text-to-image DMs [Balaji et al. 2022; Dai et al. 2023; Rombach et al. 2022a; Saharia et al. 2022b]. The SDS formulation for 3D scenes works by backpropagating gradients from a DM’s denoiser to the underlying scene representation so that the renderings look realistic. By running this optimization process over many camera views this results in a 3D consistent scene representation.

In this paper, we propose to follow this paradigm and use a pre-trained 2D inpainting DM as a prior to guide the optimization process using SDS. Concurrent works Inpaint3D [Prabhu et al. 2023] and NeRFiller [Weber et al. 2023] operate on a similar scheme, either by using the SDS objective directly or its iterative dataset update formulation proposed by IN2N [Haque et al. 2023]. We find that personalizing the DM to the target scene and reference image is key to achieving sharp results and user controllability.

Personalizing Diffusion Models Adapting large-scale text-to-image DMs to generate user-specified content offers an efficient way for obtaining a high-quality personalized generative model. This principle has been successfully applied to many applications, such as preserving the identity of an object [Ruiz et al. 2023] or rendering a chrome ball to estimate lighting [Phongthawee et al. 2023]. Different personalization approaches have been proposed; DreamBooth [Ruiz et al. 2023] finetunes a DM and Textual inversion [Gal et al. 2022] optimizes a new word embedding that can generate targets through a pretrained DM. LoRA [Hu et al. 2022; Shah et al. 2023], originally proposed for language models, injects trainable rank-decomposed matrices into frozen DMs for parameter-efficient personalization. RealFill [Tang et al. 2023] and [Chari et al. 2023] personalize both the context encoder and DM for target images.

Personalized DMs have been previously used for 2D to 3D distillation. ProlificDreamer [Wang et al. 2023a] and DreamCraft3D [Sun et al. 2023] use LoRA to learn an evolving model and compute a modified SDS objective for text-to-3D generation. Similarly, we personalize a pretrained DM using LoRA, but we propose a robust pipeline tailored for 3D inpainting to efficiently personalize the DM on an inpainted reference view and use it to inpaint a scene by optimizing an SDS objective.

3 METHOD

Our method improves the distillation of 2D DM priors for 3D inpainting of scenes represented using Gaussian splatting [Kerbl et al. 2023]. To this end, we adapt a 2D inpainting DM by employing multi-scale crops derived from a reference image (Section 3.3). The adaptation largely reduces the variance of the score distillation objective and removes the need for text guidance. Moreover, it allows us to introduce a multi-scale score distillation objective (Section 3.4) that encompasses both global context and local details. To guide the supervision of the reconstruction to the pertinent regions, we leverage the explicit nature of the Gaussian representation (Section 3.5). Important preliminaries are summarized in Section 3.1, while the implementation details are provided in Section 3.7.

3.1 Preliminaries

Diffusion Models are a family of generative models known for their ability to transform samples from a tractable distribution, typically a Gaussian, towards the target data distribution $p(\mathbf{x})$ [Ho et al. 2020; Sohl-Dickstein et al. 2015]. These models are built around two key processes. A forward process, which gradually removes the structure from the data samples $\mathbf{x} \sim p(\mathbf{x})$ by adding noise. And, a reverse process, which slowly removes this noise and reintroduces the structure into an intermediate latent variable denoted as $\mathbf{x}_t = \alpha_t \mathbf{x} + \sigma_t \epsilon$, $\epsilon \sim \mathcal{N}(\mathbf{0}, I)$. In this context, α_t and σ_t represent predetermined noise schedules, and the variable t denotes the timestep with a higher value indicating a greater amount of noise. The reverse process is typically parameterized by a conditional neural network ϵ_θ that is trained to predict the noise ϵ using the following simplified objective [Ho et al. 2020]:

$$\mathbb{E}_{\mathbf{x} \sim p(\mathbf{x}), \epsilon \sim \mathcal{N}(0, I), t \sim T} [\mathbf{w}(t) \|\epsilon_\theta(\mathbf{x}_t, t, \mathbf{c}) - \epsilon\|_2^2], \quad (1)$$

where \mathbf{c} represents a condition (e.g. text, image, etc.) that allows controlling the generation process, $\mathbf{w}(t)$ represents a time-conditional weighting, and T is a set containing a selection of timesteps.

Latent Diffusion Models (LDMs), improve computational and memory efficiency over traditional DMs by performing the diffusion process in a lower dimensional latent space [Rombach et al. 2022a]. This dimensionality reduction is achieved by employing a pretrained encoder–decoder architecture, where the encoder \mathcal{E} maps samples from the data distribution $\mathbf{x} \sim p(\mathbf{x})$ into a latent space \mathbb{Z} . The decoder \mathcal{D} performs the inverse operation, such that $\mathcal{D}(\mathcal{E}(\mathbf{x})) \approx \mathbf{x}$. In LDMs, the DM operates on \mathbb{Z} , therefore \mathbf{x} in Equation 1 is replaced by its latent representation $\mathbf{z} := \mathcal{E}(\mathbf{x})$.

Score Distillation Sampling originally proposed by [Poole et al. 2023], leverages a pretrained DM to guide the optimization of a differentiable, parametric image-rendering function $g_\phi(\pi) := \mathbf{x}$, where π denotes the camera pose from which the image \mathbf{x} is rendered. Specifically, the parameters ϕ are updated using the gradient:

$$\nabla_\phi \mathcal{L}_{\text{SDS}}(\phi, \theta) := \mathbb{E}_{\epsilon \sim \mathcal{N}(0, I), t \sim T} [\mathbf{w}(t) (\hat{\epsilon}_\theta(\mathbf{z}_t, t, \mathbf{c}) - \epsilon) \frac{\partial \mathbf{z}_t}{\partial \phi}], \quad (2)$$

where $\mathbf{z} = \mathcal{E}(g_\phi(\pi))$ and

$$\hat{\epsilon}_\theta(\mathbf{z}_t, t, \mathbf{c}) := (1 + \alpha) \epsilon_\theta(\mathbf{z}_t, t, \mathbf{c}) - \alpha \epsilon_\theta(\mathbf{z}_t, t, \emptyset). \quad (3)$$

Here, $\hat{\epsilon}_\theta$ denotes the classifier free guidance (CFG) version [Ho and Salimans 2021] of ϵ_θ used in text-conditioned DMs to enable

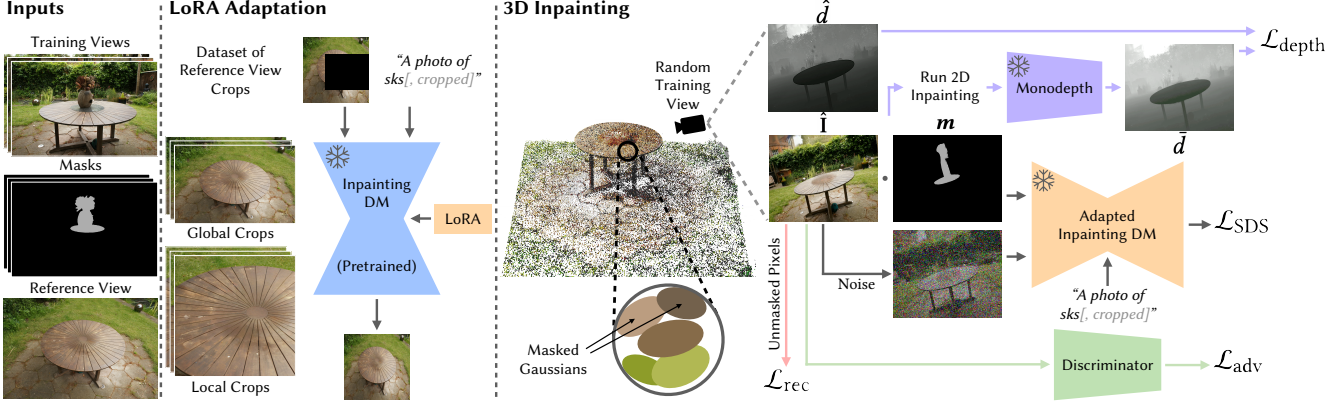


Fig. 3. Overview of the proposed approach. REFUSION takes training views, masks, and the reference view as input (*left*). We adapt the inpainting LDM on both the global and local crops of the reference view (*middle*). Then, we distill the priors of the adapted LDM to the scene (*right*) by minimizing the SDS objective. Additionally, we use a discriminator loss to mitigate potential artifacts in appearance and a depth loss to enhance geometry. We track Gaussians representing the masked and unmasked regions, and backpropagate the gradients of individual terms only to the pertinent regions.

higher quality generation via a guidance scale parameter α . Intuitively, CFG aims to trade diversity with quality and is a linear combination of two ϵ_θ terms, with the condition omitted in the latter (represented here by the null symbol \emptyset).

Personalization and Parameter Efficient Finetuning DMs can be personalized to generate images aligned with a particular concept, subject, or style [Ruiz et al. 2023; Shah et al. 2023], by finetuning their weights on a select number of images. However, updating all the parameters of a pretrained DM is computationally expensive. Instead, parameter-efficient finetuning methods like LoRA [Hu et al. 2022], inject trainable low-rank decomposition matrices and aim to learn only the variations from the pretrained weights.

Gaussian Splatting parameterizes the scene with a set of 3D Gaussian particles \mathcal{G} , where each particle is represented by its position $\mu \in \mathbb{R}^3$, scale $s \in \mathbb{R}^3$, rotation $r \in \mathbb{R}^4$, opacity $\sigma \in \mathbb{R}$, and spherical harmonics coefficients $\beta \in \mathbb{R}^{48}$. Gaussian particles can be efficiently rendered using the differentiable splatting formulation proposed in [Kerbl et al. 2023], and hence, optimized from a set of posed images using a reconstruction loss. Consequently, the set of differentiable parameters is defined as $\phi := \{\mu_i, s_i, r_i, \sigma_i, \beta_i\}_{i=1}^{|\mathcal{G}|}$.

3.2 Problem Setup

Given a 3D reconstruction of a scene and the corresponding posed images that generated it, we investigate 3D editing techniques that enable a user to perform certain manipulations. In the following, we detail our contributions on the task of 3D inpainting, before showing results on other applications that can be tackled with the same formulation Section 5. In all the experiments, we adopt Gaussian splatting [Kerbl et al. 2023] as our underlying 3D representation. However, our approach can also be applied to other 3D representations such as NeRFs [Mildenhall et al. 2020].

3.3 Multi-Scale Personalization

Our approach involves distilling the learned priors from 2D generative models into the 3D domain to provide effective generative guidance. Distilling priors from 2D image DMs into 3D using a score distillation objective is commonly recognized as a mode-seeking

optimization problem. As a result, the outputs produced by this procedure often exhibit a lack of detail and diversity. In addition, DMs are typically guided using text prompts, which are not suited to describe large-scale scenes and therefore only provide weak regularization. To mitigate these problems, we propose to personalize the DM based on a single (or multiple) reference image of the scene before distilling its priors to 3D. This personalization adapts the DM towards the reference image and alleviates the need for text guidance during the distillation process.

Let $I_r \in \mathbb{R}^{h \times w \times 3}$ denote a reference image, which can be generated by an inpainting model or an actual image of the scene. We use LoRA finetuning to personalize a pretrained inpainting LDM to I_r by minimizing the objective in Equation 1. Specifically, at each iteration, we first augment I_r by cropping out a random thin border around it to obtain $I_r^c \in \mathbb{R}^{h' \times w' \times 3}$, where $h' \leq h$ and $w' \leq w$. We then sample a random rectangular mask $m \in \{0, 1\}^{h' \times w'}$ that masks out part of the image and task the LDM to inpaint the missing content. The conditioning c in Equation 1 is obtained by concatenating the latent representation of the masked reference view $z = \mathcal{E}(m \circ I_r^c)$ and the mask m , where \circ denotes the element-wise product. For the text embedding $y = \mathcal{E}_{text}(C_T)$ we use a fixed prompt $C_T = "A photo of sks"$. We apply LoRA to the attention layers of both the text encoder \mathcal{E}_{text} and the U-Net denoiser ϵ_θ .

In practice, the native image resolution of our LDM is 512×512 pixels with a 64×64 dimensional latent space. Such low resolution is often too coarse to capture the high-frequency details of the scene. Especially, as the gradients of the SDS loss are computed in the low-resolution latent space and then backpropagated to the input (*cf.* Equation 2). To address this challenge, we propose a multi-scale personalization strategy wherein the diffusion inpainter is additionally finetuned on local 512×512 crops sampled around the masked region of I_r . To enable the DM to discern variations between local and global crops we use a distinct text prompt, $C'_T = "A photo of sks, cropped"$ for these local crops.

3.4 Multi-Scale SDS Objective

Building on the multi-scale personalization, we formulate a multi-scale SDS objective:

$$\mathcal{L}_{\text{SDS}} := \mathcal{L}_{\text{SDS}}^{\text{global}} + \mathcal{L}_{\text{SDS}}^{\text{local}}. \quad (4)$$

Specifically, consider an image $\hat{\mathbf{I}}_i$ rendered from a random camera pose from the training set along with its mask, \mathbf{m}_i . Then, $\nabla \mathcal{L}_{\text{SDS}}^{\text{global}}$ is computed using the whole $\hat{\mathbf{I}}_i$ and the text guidance "A photo of sks", while $\mathcal{L}_{\text{SDS}}^{\text{local}}$ considers only a random patch $\hat{\mathbf{I}}_i^p$ around the masked region of $\hat{\mathbf{I}}_i$ and is guided using the text prompt "A photo of sks, cropped". Such multi-scale formulation allows us to balance global context with local details even at the low resolution of the DM's latent space.

3.5 Splitting the Gaussians into Masked/Unmasked Sets

We assume that the region of the scene that should be removed and inpainted is either masked directly in 3D or provided in the form of 2D masks for each training view. The latter can be generated using an off-the-shelf 2D segmentation method or provided by the user. As such 2D masks can be inconsistent in 3D, we propose a simple heuristic that consolidates them.

3D Consistent Masks To consolidate inconsistent 2D masks, we first determine if each Gaussian particle should be masked or unmasked, by counting how often it contributes to the volume rendering of masked and unmasked pixels across the training views. If the ratio masked/unmasked is above a threshold τ_{mask} the 3D particle is labeled as masked. After particle labelling, we rasterize them back to the training views and threshold the rendered semantic values using τ'_{mask} , producing a set of 3D consistent 2D binary masks.

Confining the Loss Functions to Pertinent Regions During the optimization, we use the per-Gaussian masks to direct the gradients of individual loss terms. Specifically, the reconstruction loss from unmasked pixels only updates the parameters of unmasked Gaussians, whereas the gradients from other loss terms are only propagated to the masked Gaussians. This differentiation into masked and unmasked Gaussians is crucial to prevent guidance losses (e.g., SDS loss) from undesirably influencing the regions that do not require hallucination. But, it also requires us to adapt the densification and pruning heuristics proposed in [Kerbl et al. 2023]. Specifically, if a Gaussian is split or cloned we transfer its mask value to its children. Additionally, if a Gaussian transitions between the regions, we prune it to maintain region-specific fidelity.

Reference-Guided Initialization At the start of the inpainting process, we remove Gaussians in the masked scene region and replace them using the reference view \mathbf{I}_r . Specifically, we first predict the depth \hat{d}_r of the reference image \mathbf{I}_r . We then compensate the scale and offset ambiguities to derive the aligned depth \hat{d}_r (similar to what will follow in our depth regularization) and unproject it to 3D. We empirically observe that reference-guided initialization outperforms random initialization Table 3.

3.6 Losses and Training

We train our method using the combination of the multiscale SDS objective Section 3.4 and the reconstruction loss \mathcal{L}_{rec} ($L1$ and D-SSIM). Additionally, we employ two regularization terms that improve the

geometry and appearance of the synthesized region. The overall objective is:

$$\mathcal{L} := \mathcal{L}_{\text{rec}} + \lambda_{\text{SDS}} \mathcal{L}_{\text{SDS}} + \lambda_{\text{depth}} \mathcal{L}_{\text{depth}} + \lambda_{\text{adv}} \mathcal{L}_{\text{adv}}, \quad (5)$$

where $\lambda_* > 0$ balance the relative contribution of each loss term and \mathcal{L}_{adv} and $\mathcal{L}_{\text{depth}}$ denote the adversarial and depth loss, respectively.

Depth Regularization We regularize the depth using the outputs of a monocular depth estimation model. In particular, after every N_{depth} iterations, we render an image $\hat{\mathbf{I}}_i$ from a randomly selected camera pose in the training set. We then mask $\hat{\mathbf{I}}_i$ with its corresponding mask \mathbf{m}_i and inpaint it using our adapted inpainting model starting from a random timestep $t_{\text{depth}} \in T$. This process yields an inpainted view $\hat{\mathbf{I}}_{\text{inpaint}}$ that we feed into a monocular depth estimation model to obtain the depth map \tilde{d} .

Note that \tilde{d} is only relative and ambiguous in terms of scale and offset. To fix the ambiguity, we optimize a scale s and offset o to minimize the $L2$ error between the rendered depth, \hat{d} , and the aligned depth $\bar{d} = s\tilde{d} + o$ for the set of unmasked pixels P_{unmasked} . Finally, we employ the fast bilateral solver [Barron and Poole 2016] to reduce potential remaining misalignments and calculate $\mathcal{L}_{\text{depth}}$ on the masked pixels, P_{masked} , as:

$$\mathcal{L}_{\text{depth}} := \frac{1}{|P_{\text{masked}}|} \sum_{p \in P_{\text{masked}}} \|\hat{d}(p) - \bar{d}(p)\|_2^2. \quad (6)$$

Adversarial Objective To mitigate any color mismatches and artifacts on the boundary of the hallucinated region, we employ a discriminator \mathcal{D}_ξ parameterized by ξ . This discriminator is trained to differentiate between real patches that are sampled around the masked region of the reference view \mathbf{I}_r and the fake patches rendered from $g_\phi(\pi)$ around the mask of the training views. We propagate the gradients of the adversarial loss to all spherical harmonics coefficients $\beta_i \in \phi$, while keeping other parameters fixed. Following GANeRF [Roessle et al. 2023], we employ the following regularized version of the GAN loss \mathcal{L}_{adv} with an R_1 gradient penalty [Mescheder et al. 2018] on \mathcal{D}_ξ , controlled by a balancing scalar λ_{gp} :

$$\min_{\phi} \max_{\xi} \mathbb{E} \left[f(\mathcal{D}_\xi(\hat{\mathbf{I}}_{\text{fake}}^P)) + f(-\mathcal{D}_\xi(\mathbf{I}_{\text{real}}^P)) - \lambda_{\text{gp}} \|\nabla \mathcal{D}_\xi(\hat{\mathbf{I}}_{\text{fake}}^P)\|_2^2 \right], \quad (7)$$

where $f(x) := -\log(1 + \exp(-x))$, and $\hat{\mathbf{I}}_{\text{fake}}^P$ and $\mathbf{I}_{\text{real}}^P$ correspond to the sampled fake and real patches, respectively.

3.7 Implementation Details

For unprojection and reprojection of the masks, we set τ_{mask} and τ'_{mask} to 1 and 0.3, respectively. In each iteration, we compute $\mathcal{L}_{\text{SDS}}^{\text{global}}$ using an image rendered from a random camera pose from the training set, while averaging the $\mathcal{L}_{\text{SDS}}^{\text{local}}$ across two 512×512 patches sampled from the bounding box of the masked region. Following Gaussian splatting [Kerbl et al. 2023], we resize each training view to have the larger side of the images be 1600 pixels. The depth loss is calculated every 8th iteration. For the adversarial loss, we sample 64 real and 64 fake 64×64 patches every iteration. The architecture of the discriminator follows StyleGAN2 [Karras et al. 2020], and the hyperparameters of the adversarial loss are consistent with GANeRF [Roessle et al. 2023]. The loss weights of individual loss terms are set to $\lambda_{\text{SDS}} := 0.001$, $\lambda_{\text{depth}} := 0.0625$, and $\lambda_{\text{adv}} := 0.03$,

respectively. We adopt the Gaussian optimization parameters from [Kerbl et al. 2023], but change the *densification and cloning* heuristic to prevent overdensification of Gaussians due to larger gradients of the SDS loss. To generate the reference views we use SDXL [Podell et al. 2023] inpainting model due to its higher resolution and quality. However, to speed up the distillation, we personalize Stable-Diffusion-2-Inpainting [Rombach et al. 2022b] as the adapted LDM. The same LoRA optimization parameters as RealFill [Tang et al. 2023] are employed; we train the DM for 2000 iterations, with LoRA rank set to 8, α set to 16, resolution set to 512, and learning rates $2e^{-4}$ and $4e^{-5}$ for the U-Net and the text encoder, respectively. We set the LoRA dropout to 0.1. Note that the adapted LDM expects 512×512 images; thus, for calculating the global SDS loss, we first bilinearly downsample the rendered views to 512×512 .

4 EXPERIMENTS

Dataset and Metrics Following related work, we perform most experiments on the SPIn-NeRF [Mirzaei et al. 2023b] dataset. It consists of 10 scenes originally designed for object removal evaluation. Each scene in the dataset includes 60 images with an unwanted object (training views) and 40 images without it (test views). Human-annotated masks of the object region are available for both training and test views. For more information about the dataset please refer to [Mirzaei et al. 2023b]. To perform a quantitative comparison of our method to the selected baselines, we use 40 ground-truth images of each scene without the object. Specifically, we render corresponding views from each model and compute the average learned perceptual image patch similarity (LPIPS) [Zhang et al. 2018]¹. In line with the related work [Mirzaei et al. 2023b] we calculate the metrics around the masked region by considering the bounding box of the mask and dilating the box in every direction by 10%. To address the limitations of SPIn-NeRF dataset in demonstrating method behaviors on scenes with more significant camera motion for inpainting, we introduce our dataset comprising nine scenes. This dataset encompasses wide-baseline forward-facing scenes as well as 360-degree scenes. For each scene, our dataset includes images both with and without unwanted objects, along with human-annotated masks for every scene.

We further performed a user study using Amazon Mechanical Turk. Specifically, raters were shown videos depicting the results of two methods rendered from the same novel trajectories (our method and a baseline in random order), along with the input video and images highlighting the unwanted object. Raters were then asked to vote for the method that produced the best video in terms of *overall quality* and best *object removal*. To improve the quality of responses, we introduced an attention check task. For each scene, we added a question where the videos displayed for both methods were the same (outputs of our model) and added an option suggesting that both of the videos are identical. We set a threshold of 50% accuracy on the attention check questions to strike a balance between the quantity and quality of the responses. In total, this resulted in 32 users comparing our method to three baselines across 10 scenes and answering 2 questions per example.

¹Prior work also reports per-scene FID score, but due to the small size of the dataset (40 images) FID values are unrepresentative. We thus omit them and only report LPIPS.

Table 1. Quantitative evaluation of object removal on SPIn-NeRF dataset.

Method	LPIPS \downarrow
NeRF + LaMa (2D)	0.5369
ObjectNeRF [Yang et al. 2021]	0.6829
Masked NeRF [Mildenhall et al. 2020]	0.6030
NeRF-In [Liu et al. 2022]	0.4884
SPIn-NeRF-SD [Mirzaei et al. 2023b]	0.5701
SPIn-NeRF-LaMa [Mirzaei et al. 2023b]	0.4654
Inpaint3D [Prabhu et al. 2023]	0.5150
Reference-guided NeRF [Mirzaei et al. 2023a] (SDV2)	0.4532
Reference-guided NeRF [Mirzaei et al. 2023a] (SDXL)	0.4453
Ours	0.4283

Table 2. User study of object removal on SPIn-NeRF dataset. For each method we report the percentage of raters that preferred it over ours.

Method	Quality (%)	Removal (%)
SPIn-NeRF-LaMa	18.38	29.32
Inpaint3D	11.87	11.52
Reference-guided NeRF (SDXL)	23.64	43.65

Baselines We compare REFUSION to two naive baselines, *Masked NeRF* and *NeRF + LaMa*. In the former, the reconstruction loss is only calculated on the unmasked pixels, while the latter uses LaMa [Suvorov et al. 2022] to independently inpaint rendered views. We further compare to a wide range of existing 3D inpainting methods: ObjectNeRF [Yang et al. 2021], NeRF-In [Liu et al. 2022], SPIn-NeRF [Mirzaei et al. 2023b], and concurrent work Inpaint3D [Prabhu et al. 2023]. For all the baselines, we used the source code or the rendered images provided by the authors of the respective works.

Object Removal We first provide evaluations based on the standard 3D inpainting benchmark, the SPIn-NeRF dataset [Mirzaei et al. 2023b]. To ensure a fair comparison, we use the human-annotated masks from the SPIn-NeRF dataset for all methods. As depicted in Table 1 our method surpasses all baselines in terms of LPIPS. Furthermore, we also compare favourably in a qualitative comparison as seen in Figure 4. Note that the perceptual loss used in SPIn-NeRF doesn't fully resolve the multi-view inconsistencies introduced by inpainting each training view separately, therefore resulting in visual artifacts. Reference-guided NeRF performs well in the removal region, however the quality of the overall reconstruction quality suffers. Finally, Inpaint3D also distills a pretrained 2D inpainting DM using an SDS objective, however the lack of personalization results in a fuzzy inpainting. We summarize the results of the user study in Table 2, REFUSION outperforms all baselines in terms of *overall quality* and *object removal*.

The SPIn-NeRF dataset [Mirzaei et al. 2023b] exclusively comprises scenes with minimal camera movements. To remedy this constraint, we introduce our dataset featuring nine distinct scenes with broader camera baselines, including wide-baseline forward-facing scenes and 360-degree scenes. In Figure 5, we present qualitative comparisons between the outcomes of our approach and Reference-guided NeRF applied to scenes from the MipNeRF360 dataset [Barron et al. 2022] (depicted in the first and second scenes of the left column), as well as our own scenes. The results notably illustrate that Reference-guided NeRF, reliant solely on a single inpainted view



Fig. 4. Qualitative object removal results on the SPIn-NeRF dataset. RefFusion consistently outperforms the baselines, yielding sharper reconstruction and more plausible inpainting.

Table 3. Ablation study of object removal on SPIn-NeRF dataset.

Method	LPIPS↓
Ours w/o personalization	0.5719
Ours w/o splitting the Gaussians	0.5128
Ours w/o local SDS	0.5093
Ours w/o reference-guided initialization	0.4680
Ours w/o adversarial loss	0.4326
Ours w/o depth loss	0.4299
Ours	0.4283

for projection into 3D space, encounters challenges in extrapolating information from the reference to further views. Conversely, our method consistently yields sharper and more plausible inpainting results without visual artifacts. Note that in the third example, we remove two distinct objects by concurrently incorporating both into the masks.

Ablation on Design Choices We perform ablation studies on our key design choices to highlight their significance. Table 3 and Figure 10 depict quantitative and qualitative results. The largest drop in performance is observed when removing *personalization* from our method. This confirms our intuition that reference adaptation is crucial for unlocking the potential of SDS-based optimization at the scene level. Other ablations show that removing any components leads to adverse effects on the final outcomes. While we found the depth loss not to be crucial for the object removal task, it still contributes to a subtle improvement. Moreover, it is particularly beneficial for other applications such as object insertion.

5 APPLICATIONS

In this section, we demonstrate the general applicability of our method to various downstream 3D applications.

Sparse View Reconstruction To investigate the benefits of our method for guiding the sparse view reconstruction, we consider a scene with an unwanted occluder where only a small set of clean images from the scene (GT views) is available. Specifically, we consider two settings: a) we only use the GT views for LoRA finetuning and do not use them during the reconstruction—*Ours (LoRA)*, or b) we

additionally use the GT views for supervision using reconstruction loss—*Ours (LoRA + recon)*. Figure 6 shows that generative priors can guide the reconstruction in a sparse view setting², especially when only a small number of views are available. Indeed, *Ours (LoRA + recon)* consistently outperforms 3DGs in terms of LPIPS and PSNR. Figure 11 depicts a qualitative comparison with 3DGs.

Object Insertion Figure 7 illustrates the capacity of RefFusion to insert objects into a scene. We demonstrate that by using a reference view with an added object in the masked region, obtained using a text-to-image inpainting diffusion model. Our method succeeds in distilling the specified object into the scene with high visual fidelity.

Scene Outpainting In Figure 8, we follow the procedure proposed in [Prabhu et al. 2023] and generate inverse masks by placing a sphere at a fixed distance along the optical axis and checking for ray-sphere intersection. Example mask is shown in Figure 8 (left). Given this mask, we task our method to outpaint the scene using the same formulation and hyperparameters used for object removal. Our method completes the scene in a plausible manner, but the outpainted regions lack visual fidelity and high-frequency details. This hints that special treatment is required to obtain the same quality of results when performing outpainting.

6 CONCLUSIONS, LIMITATIONS AND FUTURE WORK

We introduced RefFusion, a 3D inpainting framework that achieves state-of-the-art results, while offering improved controllability over the inpainted content. We achieve this by personalizing an inpainting LDM to the given reference image and distilling the adapted diffusion prior to the 3D scene. We demonstrate the generality of our method across a diverse set of downstream applications including object insertion, 3D outpainting, and sparse view reconstruction.

Despite achieving notable results, there are many avenues to improve RefFusion. The primary challenge lies in removing large objects that substantially cover parts of the reference image. Fine-tuning the diffusion model on the target dataset could help bridge this gap. Additionally, although LoRA improves the efficiency of the adaptation process to the target scene, this process still requires a

²A similar observation was concurrently shown by [Wu et al. 2023].



Fig. 5. Qualitative object removal results on scenes with larger camera movements (MipNeRF360 dataset [Barron et al. 2022] and scenes from our proposed dataset). REFFUSION consistently outperforms the Reference-guided NeRF.

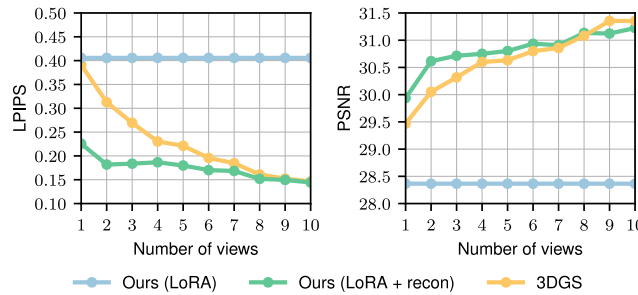


Fig. 6. Results of the sparse view reconstruction on SPIn-NeRF dataset. Using the sparse GT views only for personalization *Ours (LoRA)* already yields competitive results. When combined with the reconstruction loss *Ours (LoRA + recon)* consistently outperforms 3DGS [Kerbl et al. 2023], showcasing the potential of generative priors to guide 3D reconstruction.

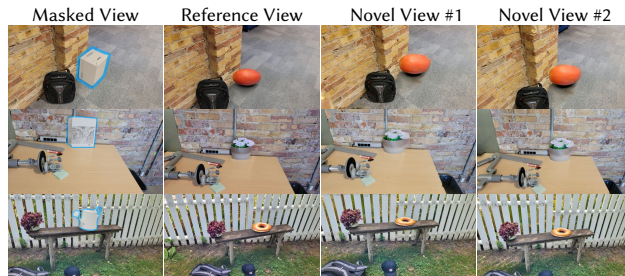


Fig. 7. Sample object insertion results.



Fig. 8. Our approach is capable of outpainting scenes by inverted masks.

considerable amount of time. Further advancements in parameter-efficient finetuning and personalization of diffusion models are expected to further speed up and enhance our approach.

Finally, recent advances in multi-view aware and video diffusion models could significantly enhance the multi-view quality of our results. Especially, as the remaining artifacts are mostly visible when the camera moves.

REFERENCES

- Omri Avrahami, Dani Lischinski, and Ohad Fried. 2022. Blended diffusion for text-driven editing of natural images. In *CVPR*.
- Yogesh Balaji, Seungjun Nah, Xun Huang, Arash Vahdat, Jiaming Song, Qinsheng Zhang, Karsten Kreis, Miika Aittala, Timo Aila, Samuli Laine, Bryan Catanzaro, Tero Karras, and Ming-Yu Liu. 2022. eDiff-I: Text-to-Image Diffusion Models with Ensemble of Expert Denoisers. *arXiv* (2022).
- Jonathan T. Barron, Ben Mildenhall, Dor Verbin, Pratul P. Srinivasan, and Peter Hedman. 2022. Mip-NeRF 360: Unbounded Anti-Aliased Neural Radiance Fields. *CVPR* (2022).
- Jonathan T Barron and Ben Poole. 2016. The fast bilateral solver. In *ECCV*.
- Miguel Ángel Bautista, Pengsheng Guo, Samira Abnar, Walter Talbott, Alexander T Toshev, Zhuoyuan Chen, Laurent Dinh, Shuangfei Zhai, Hanlin Goh, Daniel Ulbricht, Afshin Dehghan, and Joshua M. Susskind. 2022. GAUDI: A Neural Architect for Immersive 3D Scene Generation. In *NeurIPS*.
- Pradyumna Chari, Sizhu Ma, Daniil Ostashev, Achuta Kadambi, Gurunandan Krishnan, Jian Wang, and Kfir Aberman. 2023. Personalized Restoration via Dual-Pivot Tuning. *arXiv* (2023).
- Rui Chen, Yongwei Chen, Ningxin Jiao, and Kui Jia. 2023. Fantasia3D: Disentangling Geometry and Appearance for High-quality Text-to-3D Content Creation. In *ICCV*.
- Xiaoliang Dai, Ji Hou, Chih-Yao Ma, Sam Tsai, Jialiang Wang, Rui Wang, Peizhao Zhang, Simon Vandenhende, Xiaofang Wang, Abhimanyu Dubey, Matthew Yu, Abhishek Kadian, Filip Radenovic, Dhruv Mahajan, Kunpeng Li, Yue Zhao, Vladan Petrovic, Mitesh Kumar Singh, Simran Motwani, Yi Wen, Yiwen Song, Roshan Sumbaly, Vignesh Ramanathan, Zijian He, Peter Vajda, and Devi Parikh. 2023. Emu: Enhancing Image Generation Models Using Photogenic Needles in a Haystack. *arXiv* (2023).
- Rinon Gal, Yuval Alaluf, Yuval Atzmon, Or Patashnik, Amit H Bermano, Gal Chechik, and Daniel Cohen-Or. 2022. An image is worth one word: Personalizing text-to-image generation using textual inversion. *arXiv* (2022).

- Ian Goodfellow, Jean Pouget-Abadie, Mehdi Mirza, Bing Xu, David Warde-Farley, Sherjil Ozair, Aaron Courville, and Yoshua Bengio. 2014. Generative adversarial nets. *NeurIPS* (2014).
- Ayaan Haque, Matthew Tancik, Alexei Efros, Aleksander Holynski, and Angjoo Kanazawa. 2023. Instruct-NeRF2NeRF: Editing 3D Scenes with Instructions. In *ICCV*.
- Jonathan Ho, Ajay Jain, and Pieter Abbeel. 2020. Denoising Diffusion Probabilistic Models. In *NeurIPS*.
- Jonathan Ho and Tim Salimans. 2021. Classifier-free diffusion guidance. *NeurIPS Workshops* (2021).
- Edward J Hu, Yelong Shen, Phillip Wallis, Zeyuan Allen-Zhu, Yuanzhi Li, Shean Wang, Lu Wang, and Weizhu Chen. 2022. LoRA: Low-rank adaptation of large language models. *ICLR* (2022).
- Nikolai Kalischek, Torben Peters, Jan D. Wegner, and Konrad Schindler. 2022. Tetrahedral Diffusion Models for 3D Shape Generation. *arXiv* (2022).
- Tero Karras, Samuli Laine, Miika Aittala, Janne Hellsten, Jaakko Lehtinen, and Timo Aila. 2020. Analyzing and Improving the Image Quality of StyleGAN. In *CVPR*.
- Bernhard Kerbl, Georgios Kopanas, Thomas Leimkühler, and George Drettakis. 2023. 3D Gaussian Splatting for Real-Time Radiance Field Rendering. *ToG* (2023).
- Seung Wook Kim, Bradley Brown, Kangxue Yin, Karsten Kreis, Katja Schwarz, Daiqing Li, Robin Rombach, Antonio Torralba, and Sanja Fidler. 2023. NeuralField-LDM: Scene Generation with Hierarchical Latent Diffusion Models. In *CVPR*.
- Wenbo Li, Zhe Lin, Kun Zhou, Lu Qi, Yi Wang, and Jiaya Jia. 2022. Mat: Mask-aware transformer for large hole image inpainting. In *CVPR*.
- Yixun Liang, Xin Yang, Jiantao Lin, Haodong Li, Xiaogang Xu, and Yingcong Chen. 2023. LucidDreamer: Towards High-Fidelity Text-to-3D Generation via Interval Score Matching. *arXiv* (2023).
- Chen-Hsuan Lin, Jun Gao, Luming Tang, Towaki Takikawa, Xiaohui Zeng, Xun Huang, Karsten Kreis, Sanja Fidler, Ming-Yu Liu, and Tsung-Yi Lin. 2023. Magic3D: High-Resolution Text-to-3D Content Creation. In *CVPR*.
- Huan Ling, Seung Wook Kim, Antonio Torralba, Sanja Fidler, and Karsten Kreis. 2023. Align Your Gaussians: Text-to-4D with Dynamic 3D Gaussians and Composed Diffusion Models. *arXiv* (2023).
- Hongyu Liu, Ziyu Wan, Wei Huang, Yibing Song, Xintong Han, and Jing Liao. 2021. Pd-gan: Probabilistic diverse gan for image inpainting. In *CVPR*.
- Hao-Kang Liu, I Shen, Bing-Yu Chen, et al. 2022. NeRF-In: Free-form NeRF inpainting with RGB-D priors. *CGA* (2022).
- Andreas Lugmayr, Martin Danelljan, Andres Romero, Fisher Yu, Radu Timofte, and Luc Van Gool. 2022. Repaint: Inpainting using denoising diffusion probabilistic models. In *CVPR*.
- Chenlin Meng, Yang Song, Jiaming Song, Jiajun Wu, Jun-Yan Zhu, and Stefano Ermon. 2022. Sdedit: Image synthesis and editing with stochastic differential equations. *ICLR* (2022).
- Lars Mescheder, Andreas Geiger, and Sebastian Nowozin. 2018. Which training methods for GANs do actually converge?. In *ICML*.
- Ben Mildenhall, Pratul P Srinivasan, Matthew Tancik, Jonathan T Barron, Ravi Ramamoorthi, and Ren Ng. 2020. NeRF: Representing scenes as neural radiance fields for view synthesis. In *ECCV*.
- Ashkan Mirzaei, Tristan Aumentado-Armstrong, Marcus A Brubaker, Jonathan Kelly, Alex Levinstein, Konstantinos G Derpanis, and Igor Gilitschenski. 2023a. Reference-guided Controllable Inpainting of Neural Radiance Fields. *ICCV* (2023).
- Ashkan Mirzaei, Tristan Aumentado-Armstrong, Konstantinos G Derpanis, Jonathan Kelly, Marcus A Brubaker, Igor Gilitschenski, and Alex Levinstein. 2023b. SPIn-NeRF: Multiview segmentation and perceptual inpainting with neural radiance fields. In *CVPR*.
- Alex Nichol, Heewoo Jun, Prafulla Dhariwal, Pamela Mishkin, and Mark Chen. 2022. Point-E: A System for Generating 3D Point Clouds from Complex Prompts.
- Pakkapon Phongthawee, Worameth Chinchuthakun, Nontaphat Sinsunthithet, Amit Raj, Varun Jampani, Pramook Khungurn, and Supasorn Suwajanakorn. 2023. DiffusionLight: Light Probes for Free by Painting a Chrome Ball. *arXiv* (2023).
- Dustin Podell, Zion English, Kyle Lacey, Andreas Blattmann, Tim Dockhorn, Jonas Müller, Joe Penna, and Robin Rombach. 2023. SDXL: Improving Latent Diffusion Models for High-Resolution Image Synthesis. *arXiv* (2023).
- Ben Poole, Ajay Jain, Jonathan T. Barron, and Ben Mildenhall. 2023. DreamFusion: Text-to-3D using 2D Diffusion. *ICLR* (2023).
- Kira Prabhu, Jane Wu, Lynn Tsai, Peter Hedman, Dan B Goldman, Ben Poole, and Michael Broxton. 2023. Inpaint3D: 3D Scene Content Generation using 2D Inpainting Diffusion. *arXiv* (2023).
- Jiawei Ren, Liang Pan, Jiaxiang Tang, Chi Zhang, Ang Cao, Gang Zeng, and Ziwei Liu. 2023. DreamGaussian4D: Generative 4D Gaussian Splatting. *arXiv* (2023).
- Barbara Roessle, Norman Müller, Lorenzo Porzi, Samuel Rota Bulò, Peter Kortschieder, and Matthias Nießner. 2023. GANeRF: Leveraging Discriminators to Optimize Neural Radiance Fields. *ToG* (2023).
- Robin Rombach, Andreas Blattmann, Dominik Lorenz, Patrick Esser, and Björn Ommer. 2022a. High-Resolution Image Synthesis with Latent Diffusion Models. In *CVPR*.
- Robin Rombach, Andreas Blattmann, Dominik Lorenz, Patrick Esser, and Björn Ommer. 2022b. High-Resolution Image Synthesis With Latent Diffusion Models. In *CVPR*.
- Nataniel Ruiz, Yuanzhen Li, Varun Jampani, Yael Pritch, Michael Rubinstein, and Kfir Aberman. 2023. DreamBooth: Fine Tuning Text-to-image Diffusion Models for Subject-Driven Generation. (2023).
- Chitwan Saharia, William Chan, Huiwen Chang, Chris Lee, Jonathan Ho, Tim Salimans, David Fleet, and Mohammad Norouzi. 2022a. Palette: Image-to-image diffusion models. In *SIGGRAPH*.
- Chitwan Saharia, William Chan, Saurabh Saxena, Lala Li, Jay Whang, Emily Denton, Seyed Kamyar Seyed Ghasempour, Raphael Gontijo-Lopes, Burcu Karagol Ayan, Tim Salimans, Jonathan Ho, David J. Fleet, and Mohammad Norouzi. 2022b. Photorealistic Text-to-Image Diffusion Models with Deep Language Understanding. In *NeurIPS*.
- Viraj Shah, Nataniel Ruiz, Forrester Cole, Erika Lu, Svetlana Lazebnik, Yuanzhen Li, and Varun Jampani. 2023. ZipLoRA: Any Subject in Any Style by Effectively Merging LoRAs. *arXiv* (2023).
- Jascha Sohl-Dickstein, Eric Weiss, Niru Maheswaranathan, and Surya Ganguli. 2015. Deep Unsupervised Learning using Nonequilibrium Thermodynamics. In *JMLR*.
- Yang Song, Jascha Sohl-Dickstein, Diederik P Kingma, Abhishek Kumar, Stefano Ermon, and Ben Poole. 2021. Score-Based Generative Modeling through Stochastic Differential Equations. In *ICLR*.
- Jingxian Sun, Bo Zhang, Ruizhi Shao, Lizhen Wang, Wen Liu, Zhenda Xie, and Yebin Liu. 2023. Dreamcraft3d: Hierarchical 3d generation with bootstrapped diffusion prior. *arXiv* (2023).
- Roman Suvorov, Elizaveta Logacheva, Anton Mashikhin, Anastasia Remizova, Arsenii Ashukha, Aleksei Silvestrov, Naejin Kong, Harshith Goka, Kiwoong Park, and Victor Lempitsky. 2022. Resolution-robust large mask inpainting with fourier convolutions. In *WACV*.
- Luming Tang, Nataniel Ruiz, Chu Qinghao, Yuanzhen Li, Aleksander Holynski, David E Jacobs, Bharath Hariharan, Yael Pritch, Neal Wadhwa, Kfir Aberman, and Michael Rubinstein. 2023. RealFill: Reference-Driven Generation for Authentic Image Completion. *arXiv* (2023).
- Dongqing Wang, Tong Zhang, Alaa Abboud, and Sabine Süsstrunk. 2023b. Inpaint-NeRF360: Text-Guided 3D Inpainting on Unbounded Neural Radiance Fields. *arXiv* (2023).
- Zhengyi Wang, Cheng Lu, Yikai Wang, Fan Bao, Chongxuan Li, Hang Su, and Jun Zhu. 2023a. ProlificDreamer: High-Fidelity and Diverse Text-to-3D Generation with Variational Score Distillation. In *NeurIPS*.
- Ethan Weber, Aleksander Holynski, Varun Jampani, Saurabh Saxena, Noah Snavely, Abhishek Kar, and Angjoo Kanazawa. 2023. NeRFiller: Completing Scenes via Generative 3D Inpainting. *arXiv* (2023).
- Silvan Weder, Guillermo Garcia-Hernando, Aron Monszpart, Marc Pollefeys, Gabriel J Brostow, Michael Firman, and Sara Vicente. 2023. Removing objects from neural radiance fields. In *CVPR*.
- Rundi Wu, Ben Mildenhall, Philipp Henzler, Keunhong Park, Ruiqi Gao, Daniel Watson, Pratul P. Srinivasan, Dor Verbin, Jonathan T. Barron, Ben Poole, and Aleksander Holynski. 2023. ReconFusion: 3D Reconstruction with Diffusion Priors. *arXiv* (2023).
- Shaoan Xie, Zhifei Zhang, Zhe Lin, Tobias Hinz, and Kun Zhang. 2023. Smartbrush: Text and shape guided object inpainting with diffusion model. In *CVPR*.
- Bangbang Yang, Yinda Zhang, Yinghai Xu, Yijin Li, Han Zhou, Hujun Bao, Guofeng Zhang, and Zhaopeng Cui. 2021. Learning Object-Compositional Neural Radiance Field for Editable Scene Rendering. In *ICCV*.
- Jiahui Yu, Zhe Lin, Jimei Yang, Xiaohui Shen, Xin Lu, and Thomas S Huang. 2019. Free-form image inpainting with gated convolution. In *ICCV*.
- Xiaohui Zeng, Arash Vahdat, Francis Williams, Zan Gojcic, Or Litany, Sanja Fidler, and Karsten Kreis. 2022. LION: Latent Point Diffusion Models for 3D Shape Generation. In *NeurIPS*.
- Richard Zhang, Phillip Isola, Alexei A Efros, Eli Shechtman, and Oliver Wang. 2018. The Unreasonable Effectiveness of Deep Features as a Perceptual Metric. In *CVPR*.
- Shengyu Zhao, Jonathan Cui, Yilun Sheng, Yue Dong, Xiao Liang, Eric I Chang, and Yan Xu. 2021. Large scale image completion via co-modulated generative adversarial networks. *ICLR* (2021).
- Haitian Zheng, Zhe Lin, Jingwan Lu, Scott Cohen, Eli Shechtman, Connelly Barnes, Jiamming Zhang, Ning Xu, Sohrab Amirghodsí, and Jiebo Luo. 2022. Image inpainting with cascaded modulation GAN and object-aware training. In *ECCV*.
- Yufeng Zheng, Xueling Li, Koki Nagano, Sifei Liu, Otmar Hilliges, and Shalini De Mello. 2023. A unified approach for text-and image-guided 4d scene generation. *arXiv* (2023).

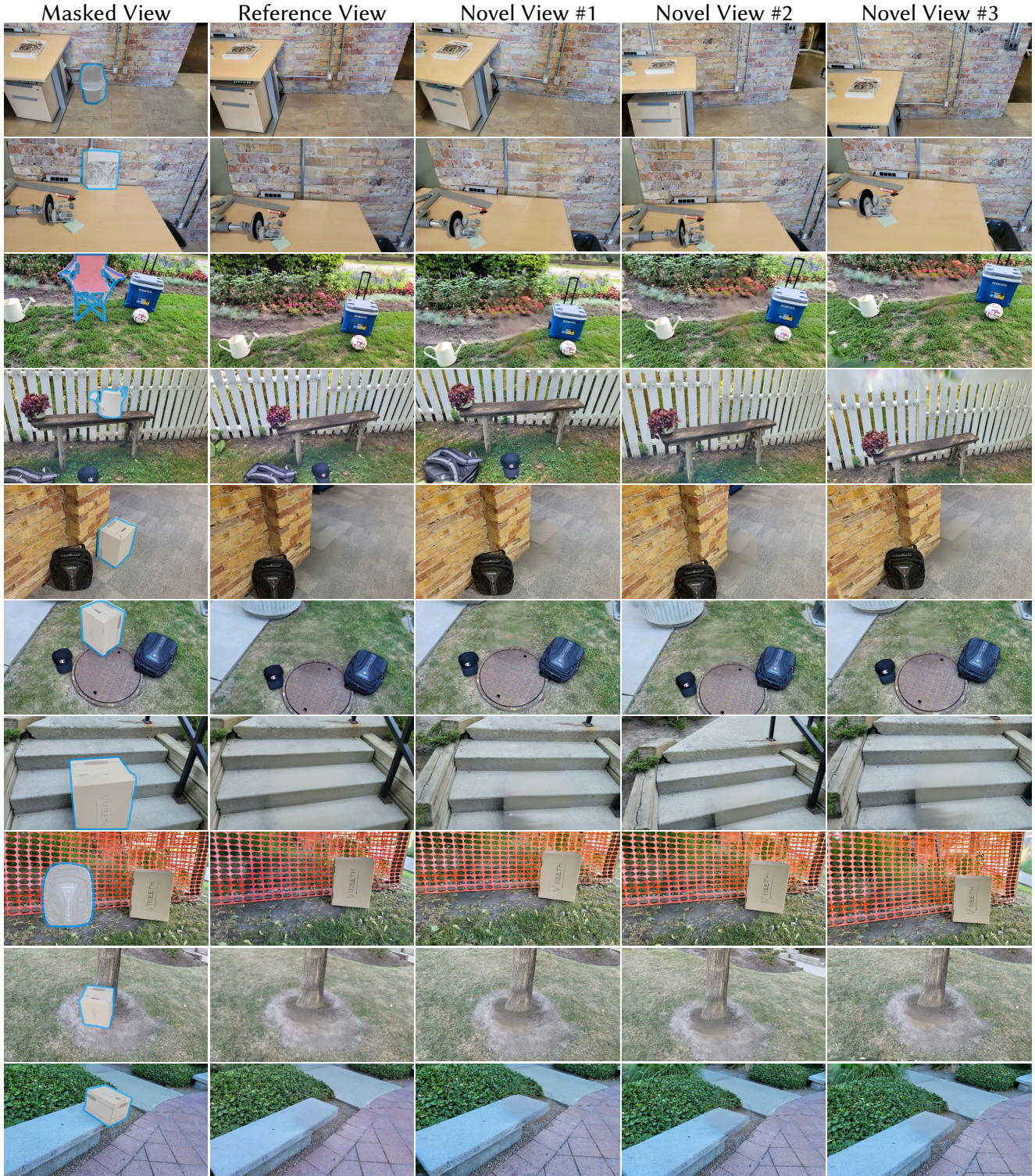


Fig. 9. Qualitative object removal results on the SPIn-NeRF dataset. REFFUSION synthesizes plausible content that is highly multi-view consistent.



Fig. 10. Qualitative results of the ablation study on SPIn-NeRF dataset. Note how different components of our method help improve different types of artifacts.

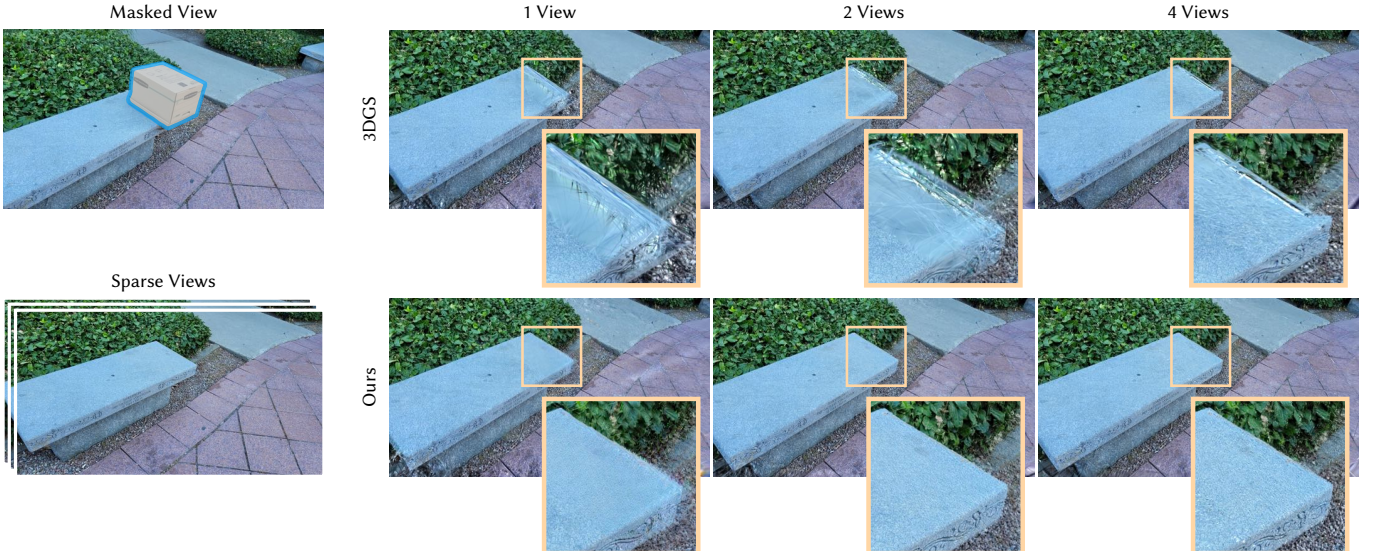


Fig. 11. Qualitative evaluation of sparse view reconstruction on SPIn-NeRF dataset. Both REFfusion and 3DCS use the reconstruction loss on sparse input images in the masked region. Additionally, REFfusion uses generative priors of the reference adapted LDM through SDS losses as well as the depth and adversarial regularization terms. Note how generative priors can successfully guide the reconstruction even in the extreme case of a single GT view.